RSC Advances




ROYAL SOCIETY OF CHEMISTRY

www.rsc.org/advances

# Ion size, loading, and charge determine the mechanical properties, surface apatite, and cell growth of silver and tantalum doped calcium silicate

Seyed Farid Seyed Shirazi[1, 2], Samira Gharehkhani[1], Hendrik Simon Cornelis Metselaar[1], Bahman Nasiri-Tabrizi[3], Hooman Yarmand[1], Mahdi Ahmadi[4], Noor Azuan Abu Osman[2]

[1] Department of Mechanical Engineering, Faculty of Engineering and Advanced Material Research Center, University of Malaya, 50603 Kuala Lumpur, Malaysia

[2] Department of Biomedical Engineering, Faculty of Engineering, University of Malaya, 50603 Kuala Lumpur, Malaysia

[3] Advanced Materials Research Center, Materials Engineering Department, Najafabad Branch, Islamic Azad University, Najafabad, Iran

[4] School of Aerospace, Mechanical and Manufacturing Engineering, RMIT University, Melbourne, Australia

Address correspondence to: faridsh80@gmail.com (Seyed Farid Seyed Shirazi)

s_gharahkhani_248@yahoo.com (Samira Gharehkhani)

Tel: 0060-14-2646276

Fax: 0060-3-79675317

**Abstract**

This study describes how various loadings of two ions with different size and charge, such as silver and tantalum, can affect the mechanical and biological properties of calcium silicate (CS). The incorporation of 5 wt% tantalum (Ta, charge: $5^+$, ion radius: 0.68 Å) in the CS lattice raised the hardness and fracture toughness values significantly. Increasing the Ta concentration to 10 wt% and 15 wt%, did not lead to further improvements. Additions of silver (Ag, charge: $1^+$, ion radius: 1.13 Å) to 5, 10 and 15 wt%, resulted in an increase in hardness and fracture toughness values in comparison to undoped CS; however, these values did not change significantly with different concentrations of Ag. Both Ta and Ag doped CS formed surface layers of apatite in simulated body fluid (SBF). CS was found to stimulate hFOB proliferation. The incorporation of Ta into CS did not change this and hFOB proliferation was stimulated even at higher concentrations. With increasing Ag content in the CS structure, the cell proliferation was slightly inhibited.

**Keywords:** Calcium silicate, Ion-exchange, silver, Tantalum, Fracture toughness, Cell proliferation

## 1. Introduction

Since the discovery of bioglass® and its biological properties [1], many researchers have studied the development of silicate bioceramics as a potential material for biomedical applications. Calcium silicate (CS, $CaSiO_3$) is a bioactive silicate ceramic that has been widely employed in coating/films, bone replacement and tissue applications in recent decades[2-3]. All relevant studies showed that CS is able to form an apatite layer on its surface by soaking in simulated body fluid (SBF) [4-5] or in human saliva [6]. Furthermore, it has been proven that cell proliferation, attachment rate and alkaline phosphates (ALP) activity were improved in implants and tissues fabricated from CS compared to hydroxyapatite (HA) ceramic [7-8]. Due to a number of disadvantages of ceramics, mostly brittleness and inadequate biological properties, insertion of implants to replace injured parts often brings about some discomfort for patients [9]. Most studies have shown that making a composite of a bioactive ceramic with reinforcement agents can remarkably enhance the mechanical properties of the ceramic matrix but in most cases, interfacial reactions between the matrix and reinforcement agents during the high temperature processing result in the formation of new phases, which affect the mechanical and biological properties [10]. To prevent possible drawbacks, it is essential to find an approach to improve the mechanical and biological properties while avoiding interfacial reactions. Substitution of metallic cations for a fraction of the calcium ions ($Ca^{2+}$) is an appropriate way to overcome some intrinsic properties of bioactive ceramic implants. So far numerous studies regarding divalent and trivalent dopants into the bioactive ceramics and carbonaceous structure have been reported[11-13]. Doping HA with divalent $Mg^{2+}$ displayed enhanced osteoblast cell proliferation compared to undoped HA [14]. It also has been found that Zinc ions ($Zn^{2+}$) can significantly increase the cell adhesion and antibacterial properties of HA[14-15]. Doping with $Cu^{2+}$ showed that besides the improvement of corrosion properties, apatite formation onto the surface of HA and CS was stimulated[15-16]. Several studies have described monovalent $Ag^{+}$ doped HA ceramic. This dopant is widely used in medicine as antibacterial agent showing an oligodynamic effect with a minimal development in the target microorganism [17]. Low concentrations of Ag are non-toxic to mammals, but higher amounts lead to cytotoxicity and argyria [18-20]. Tantalum is a metal element well known for its suitable biological and

mechanical properties [21]. Despite its unique properties, only a few studies have been focused on bioactive ceramics employing Ta cations ($Ta^{5+}$) as dopants [22].

One of the reported problems associated with ceramic implants is the presence of defects such as cracks due to post processing conditions and the brittleness of ceramics that is an intrinsic property of this class of materials. To suppress this problem some high-tech fabrication processes such as hot isostatic pressing (HIP), spark plasma sintering (SPS) and selective laser sintering (SLS) have been employed [23-24]. Incorporation of metals into a ceramic matrix is aimed at taking advantage of the ductility of metal based on a crack-bridging toughening mechanism [25]. According to a different theory the higher thermal expansion coefficient of metals can introduce stress into the ceramic matrix, therefore imparting higher toughness [26]. Over the past decades, various chemical synthesis methods have been reported for doping ceramics with metal ions. Both wet chemical process [27-29] and solid state reaction [30-31] have been used for cation and anion dopants. The mechanochemical technique is a synthesis process that has been used for the production of a wide range of materials [32-33]. This technique can produce nanocrystalline structures without the necessity for high temperature treatment and also without undesirable side-reaction, has a quite short synthesis time and often avoid the need to wash the synthesized powder. Up to now, many studies have been devoted to the synthesis of nano-crystalline materials but only few have addressed the ion substitutions in the main matrix.

The present study is aimed at the evaluation of biological behaviors and mechanical properties of calcium silicate doped with pentavalent tantalum ($Ta^{5+}$) and monovalent silver ($Ag^{+}$) introduced in a prior publication [34]. Mechanical properties including hardness and fracture toughness and biological properties as well as e.g. apatite formation and cell proliferation were assessed for various concentrations of Ag and Ta with the aim of using doped CS materials in bone implantations.

## 2. Materials and Methods

### 2.1 Preparation and characterization of Ta and Ag doped CS

Doped CS powders containing 0, 5, 10 and 15 wt% of Ta and Ag reagents ($TaCl_5$ and $AgNO_3$ respectively) were synthesized by mechanochemical method as reported in our previously published study [34]. In summary, commercial grade calcium oxide (CaO, AJAX FINECHEM), silicon dioxide gel ($SiO_2$, SIGMA ALDRICH), silver nitrate ($AgNO_3$, FLUKA) and tantalum chloride ($TaCl_5$, ACROS ORGANIC) were used as reagents without further purification. Ta and Ag dopants were used to replace calcium in CS. In accordance with the stoichiometry of calcium silicate, the mole ratios of (Ca+Ag)/Si and (Ca+Ta)/Si were equal to 1. The degree of substitution of $Ca^{2+}$ by $Ag^{+}$ was shown by the *x* value in the formula of Ag doped CS ($Ca_{1-x}Ag_xSiO_{3-x/2}$), where *x* values were selected equal to 0, 0.05, 0.10 and 0.15 and accordingly the experimental outcomes were labeled as ACS0, ACS5, ACS10 and ACS15, respectively. In a similar trend, the level of replacement of $Ca^{2+}$ by $Ta^{5+}$ was demonstrated by the *y* value in $Ca_{1-y}Ta_ySiO_{(2+3y/2)}$ formula, where *y* values were chosen equal to 0 (TCS0), 0.05 (TCS5), 0.10 (TCS10) and 0.15 (TCS15).

To prepare the ceramic disks, doped CS powders were uniaxially pressed at 250 MPa to get doped CS precursor discs with a diameter of 5mm and a height of 3mm. Subsequently, the green disks were conventionally sintered at 1200°C for 3h with a heating rate of 5°C/min to obtain the ceramic discs. Finally, the sintered discs were molded with epoxy resin before their mechanical properties were measured. The surfaces of the sintered specimens were ground with 600, 1200 and 2000 grit SiC paper, followed by polishing with 9, 3 and 0.5 µm polishing compounds to obtain a consistent surface roughness for all samples.

Microstructural characterization of the sintered doped CS discs was performed using a high resolution FEI Quanta 200F field emission scanning electron microscopy (FESEM). Energy dispersive X-ray spectroscopy (EDX) coupled to the FESEM machine was employed to image the elemental distribution in a fine structure. X-ray diffraction (XRD) of the powders and composites was performed using a

PANalytical's Empyrean XRD with mono-chromated Cu-$K_\alpha$ radiation ($\lambda$ = 1.54056 Å), operated at 45 kV, 40 mA, a step size of 0.026° and a scanning rate of 0.1°$s^{-1}$ over a 2$\theta$ range from 20° to 60°.

Phase volume fraction ($W_P$, %) was determined using semi-quantitative XRD analysis by comparing the peaks of β-CS (-3 2 0), and α-CS ((1 1 2), (-1 2 2), and (3 0 1)) from XRD patterns [35]:

$$W_P = \frac{(I)_P}{\sum_{i=1}^{n}(I)_i} \times 100 \quad \text{(I)}$$

where $(I)_P$ and $(I)_i$ are the intensity of the major peak of the phase and intensity of major peaks of all phases.

### 2.2 Evaluation of Mechanical Properties

Hardness was measured using a Vickers hardness test (MITUTOYO-AVK C200-AKASHI CORPORATION) at room temperature using an applied load of 2 kgf with a dwell time of 15 s.

Five indentations were made per sample and the average reported. The fracture toughness was calculated using the widely used Anstis model. In this method the fracture toughness is calculated from the crack length, hardness of material and also applied load according to the following equation [36-38];

$$K_{IC} = 0.0937 \times \sqrt{\frac{H_V \times P}{4 \times C}} \quad \text{(II)}$$

where, P is the applied indentation load and C is the total length of crack produced at the indentation corners from the micro-indentation tests.

### 2.3 Ability of doped CS ceramics to form an apatite layer

Simulated body fluid, SBF, containing ion concentrations similar to those in human blood plasma was prepared according to the method described by Kokubo [39]. In brief, reagent-grade $CaCl_2$, $K_2HPO_4 \cdot 3H_2O$,

NaCl, KCl, $MgCl_2 \cdot 6H_2O$, $NaHCO_3$, and $Na_2SO_4$ were dissolved in distilled water and the pH adjusted to 7.3.

The polished specimens were incubated in 10 mL SBF solution in a laminar flow hood. The samples were kept in SBF solution for 7 days and 14 days at a constant temperature of 37°C and at a pH of 7.3, with HCl and NaOH to adjust the pH. After a pre-set time point, the samples were removed and were rinsed in ethanol; then, they were analyzed by the FESEM and XRD spectrum to determine the apatite formation on the surface of each sample.

### 2.4 Dissolution rate of doped ceramics in SBF

The changes in the concentrations of the Ag, Ca, and Si ions in the SBF solution were observed after soaking the specimens for a period of time using inductive-coupled plasma atomic emission spectroscopy (Perkin Elmer, Optima 3000DV, USA).

### 2.5 Human fetal osteoblast (HFOB) cell culture

HFOB 1.19 cell lines derived from HOB was purchased from ATCC. Cells were maintained and propagated in DME/F-12 (HyClone, UT) cell culture medium supplemented with 10% fetal bovine serum (Gibco, NY), 100 U/mL penicillin and 100 mg/mL streptomycin at 37°C in a humidified atmosphere with 5% CO2.The ability of the attachment and proliferation of the cells (ATCC) on Ta doped CS ceramics were examined by culturing the cells onto composite discs. To accomplish a cell culture test, the sintered discs were sterilized in an autoclave for 20 min followed by washing by sterile PBS to remove all residues. In the next step, the samples were washed with the cell culture medium prior to their placement in a 96-well tissue culture plate (NUNC, Denmark). The cells were then cultured using cells that were seeded in wells of cell culture plates (NUNC, Denmark) that contained prepared composite discs at a density of $1\times10^4$ cells/well. A cell proliferation test was performed by a methyl thiazoletetrazodium (MTT) assay. A solution with 5mg/ml MTT in PBS was prepared. The solution was filtered through a

filter with 0.2 mm pore size and was then stored at 220°C. All specimens were soaked in the cell culture medium for 12 h after sterilization in order to stabilize the pH, before they were transferred to the cell culture microplate followed by cell seeding. At 1, 3, and 5 days post cell seeding, 20 mL MTT was added to each well. The cells were then incubated at 37°C for 4 h in a humidified atmosphere with 5% CO2. After 4 h of incubation, 100 mL of stop solution was added to the wells, and the optical density (OD) of each well was read at 570 nm using a 96 well plate reader (TECAN, Mannendorf, Switzerland).

To investigate the cell adhesion by FESEM (Ultra-high Resolution SEM SU8000, Hitachi, Japan), the cells were fixed on the surface of the composites by incubating the discs/cells construct in 4% glutaraldehyde for 12 h followed by washing the samples with PBS (0.1 M) three times and dehydration with a series of graded ethanol/water solutions (40%, 50%, 60%, 70%, 80%, 90%, and 3×100%, respectively). Next, 0.5 mL of hexamethyldisilazane (HMDS) was added to each well, including the dehydrated samples, to preserve the original morphology of the cells. Three samples of each doping concentration were tested, and each test was conducted in triplicate ($p$ -value<0.05).

## 3 Results and Discussion

### 3.1 Structural Characterization and Physical Properties

Figure 1 confirms that during the sintering process, Ta doped CS powders transformed into biphasic mixtures of α- and β-CS. Table 1 indicates the phase volume fraction (PVF, %) of the milled samples with different degrees of Ag and Ta substitutions after sintering treatment. In the absence of metallic dopants, the values of β and α-CS were 20±1% and 80±3%, respectively.

Compared to pure CS, the intensities of α-CS reflections in sintered TCS5 samples were reduced with an obvious increase in the intensities of β-CS. With increased incorporation of Ta (TCS10 and TCS15), a slight further reduction in intensities of α- phase was observed indicating less phase transformation from β to α. Based on the JCPDS 43-1460 the main reflection of β-CS at 29.98° (2 Theta) had a significantly increased intensity with higher amounts of Ta substitution. The intensities of all Ta doped samples after

sintering at 1200°C showed that further Ta substitutions retarded phase transformation to α-CS, which could be related to the heating and cooling rate of sintering[40].

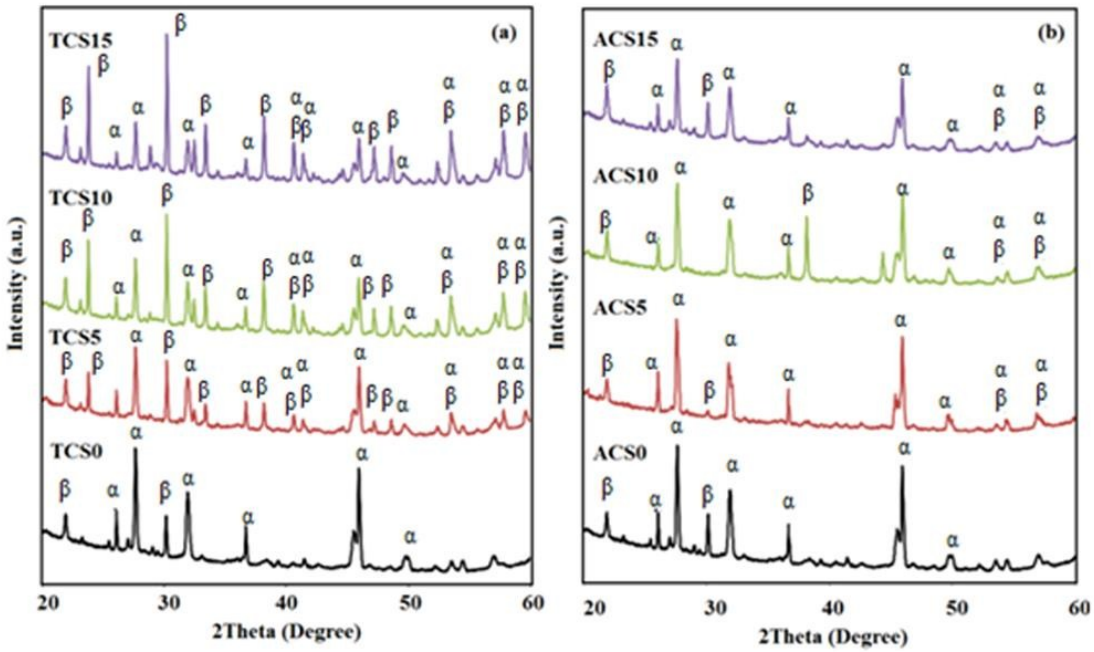


Figure 1 XRD patterns of (a) TCS and (b) ACS samples sintered at 1200°C for 2h. β and α are the index of β-CS and α-CS respectively.

In addition, it seemed that the temperature of phase transformation increased with higher Ta content, which held true for both calcinations [34] and sintering. To stabilize the β form as the dominant phase, the heating and cooling rates must be decreased. If β is the preferred phase over α heating and cooling rates should be increased. β-CS is suitable when a higher fracture toughness is desired, however transformation to α-CS leads to greater hardness [10].

ACS5 and ACS10 had an increased amount of α phase present in accordance with JCPDS 031-0300, but the intensity of β phase was higher in sintered ACS15 (Figure 1b). The intensities of α reflection in ACS15 were slightly lower than those for pure CS which could be due to disruptions of the long range order by addition of Ag contents of more than 10 wt%.

Table 1 PVF (%) as a function of β- and α-CS main reflections in comparison to undoped CS after sintering at 1200°C for 2h

| Composite Name | $W_P$ | | | |
|---|---|---|---|---|
| | β-CS | | α-CS | |
| | (-3 2 0) | (1 1 2) | (-1 2 2) | (3 0 1) |
| **CS** | 20.3±1.5 | 50.2±3.1 | 5.2±0.1 | 25.3±4.2 |
| **TCS5** | 36.5±2.2 | 42.4±1.2 | 2.1±0.2 | 20.1±1.1 |
| **TCS10** | 48.1±1.2 | 26.7±1.3 | 1.3±0.1 | 23.9±1.1 |
| **TCS15** | 59.8±3.1 | 20.4±2.2 | 1.2±0.2 | 18.8±1.2 |
| **ACS5** | 3.2±0.1 | 47.3±2.4 | 26.4±2.3 | 24.3±1.2 |
| **ACS10** | 2.4±0.2 | 59.9±3.2 | 1.9±0.2 | 36.3±1.9 |
| **ACS15** | 18.9±1.2 | 40.2±0.9 | 3.2±0.1 | 37.9±1.1 |

Recently, it was shown that the incorporation of cations with a larger ionic radius, e.g. strontium ($Sr^{2+}$), increased the crystal dimension, which may result in enhancing the transport of atoms and stimulating the phase transition of CS [41]. Hence, it is a rational expectation that Ag ions, which possess a larger ionic radius, could stimulate phase transformation due to lattice distortion. It seems that 15% Ag could create a distortion in the CS lattice, which prevented the phase transformation as observed in ACS5 and ACS10. Furthermore, it is concluded that the temperature of phase transformation for ACS15 should be much higher than for ACS5 and ACS10 due to the lower amount of vacancies in the lattice of CS, which could cause the transport of atoms and accelerated phase transition.

Previously, it was shown that the incorporation of some foreign ions in titanium dioxide ($TiO_2$) can stimulate the phase transformation from anatase to rutile, which was attributed to the formation of oxygen vacancies that enhanced the transport of atoms and accelerated the phase transformation [42].

The results revealed that both dopants changed the density of sintered samples (Table 2). Increased densification occurred in the Ag doped samples with increasing addition of Ag as the radius of $Ag^{+}$ ions is larger than that of $Ca^{2+}$. Cho, Park, Kim and Chung [43] found that $Cd^{2+}$ as a sintering additive promoted the densification of $(Pb_{0.52}Ti_{0.48})ZrO_3$ ceramics through the replacement of $Pb^{2+}$ by $Cd^{2+}$. It is reasonable to speculate that the mechanisms by which Ag induced densification of the CS ceramics, may be related to this finding and that Ag ions cause an increase in crystal dimensions, thereby enhancing the transport of atoms and accelerating the densification of CS ceramics.

Table 2 Density and porosity of doped and pure CS after sintering at 1200°C for 2h

| Composite Name | Density (g/Cm$^3$) | Porosity (%) | Grain size (μm) |
|---|---|---|---|
| **CS** | 2.40±0.06 | 17.2±0.7 | 0.24±0.04 |
| **TCS5** | 2.86±0.08 | 3.6±0.5 | 0.14±0.03 |
| **TCS10** | 2.77±0.03 | 4.8±0.5 | 0.21±0.06 |
| **TCS15** | 2.75±0.05 | 5.2±0.2 | 0.24±0.05 |
| **ACS5** | 2.47±0.1 | 14.8±0.5 | 0.25±0.03 |
| **ACS10** | 2.56±0.07 | 8.5±0.8 | 0.27±0.03 |
| **ACS15** | 2.68±0.07 | 7.7±0.3 | 0.31±0.03 |

Ta doped CS specimens showed similar densification behavior as was observed in Ag doped samples. In all cases the density of Ta-doped CS was higher than that of pure CS samples. With incorporation of 5% of Ta, the porosity of the sintered bodies decreased from 17.20±0.7% for pure CS to 3.6±0.5%, while with increasing the content of Ta up to 15 wt% this value was slightly raised to 5.2±0.2%. The results were in full agreement with the hypothesis that the densification rate depended on the radii of ions doped; i.e., the smaller the ionic radii, the better the densification rate [44]. In similar studies, rare earth doping of alumina significantly improved the densification behavior[45].

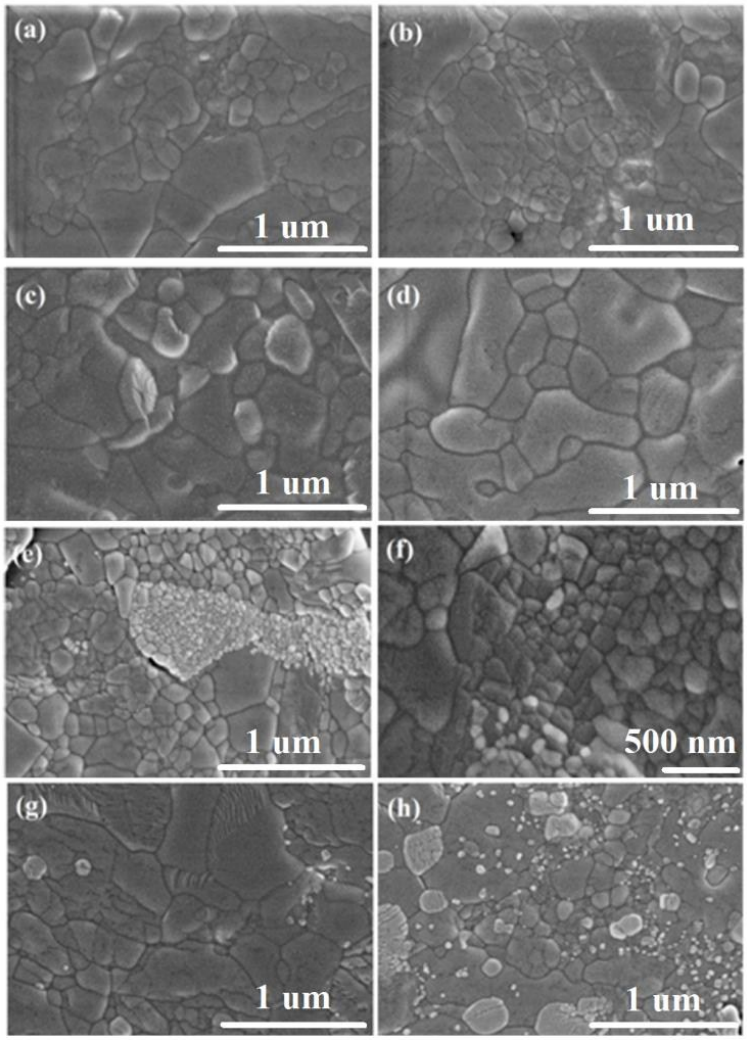


Figure 2 FESEM images of Grain size of (a) pure CS (b) ACS5 (c) ACS10 (d) ACS15 (e and f) TCS5 (g) TCS10 and (h) TCS15 sintered at 1200°C for 2h.

However, at 10 wt% and 15 wt% concentration, Ta could cause further vacancies in the CS lattice leading to the formation of a loose structure, which resulted in a lower density compared to 5 wt% Ta containing CS ceramics. As the ionic radius of Ta is smaller than Ag, Ta had more influence on the densification rate of CS in doped samples than Ag. Even though Ta has a smaller ion radius than Ag, the charge imbalance created in the CS lattice by doping with Ta increased the vacancy concentration, which most probably enhanced the transport of atoms and accelerated the densification of CS materials.

With the replacement of 10 wt% and 15 wt% Ag for Ca in the sintered samples, grain growth occurred by over a factor of two compared to undoped CS samples as shown in Table 2 and Figure 2. As can be seen from the FESEM images and the grain size analysis, the different amounts of dopants had a direct effect on the grain growth. Significant grain refinement occurred for TCS5 specimens, where the grain sizes were reduced by over 40% relative to the pure CS.

$Ta^{5+}$ as a pentavalent dopant generates charge-compensating oxygen vacancies which together with the association energy contributed and furthered the size misfit [34]. Accepting the hypothesis that oxygen vacancies enhance cation diffusion [46], it is expected that fewer oxygen vacancies were associated with $Ta^{5+}$, and that $Ta^{5+}$ had the lowest diffusivity itself and, therefore, effected the lowest grain boundary mobility. With $Ag^{+}$ doping there were not sufficient oxygen vacancies to be associated with Ag to cause significant cation diffusion and induce associated mobility at the grain boundaries. When further dopant was incorporated into CS, there was less cation diffusion, due to the lower amounts of oxygen vacancies afforded by the dopants. This caused the mobility in the doped materials to drop further and finally increased grain growth.

### 3.2 Mechanical Properties

Table 3 lists the mechanical properties including hardness, fracture toughness and Young's modulus of pure and doped CS specimens sintered at 1200°C for 2h. The hardness of pure CS is 2.57±0.13 GPa after sintering at 1200°C for 2h. The addition of Ag led to an increase of the hardness to 4.30±0.17 GPa, 4.52±0.11 GPa and 4.91±0.17 GPa for ACS5, ACS10 and ACS15, respectively. This increase may be explained from the higher density of the doped materials.

Since the hardness technique is purely a surface technique and as such the hardness of a material is dependent on the physical characteristics of the surface [47,48], it is likely that the level of surface porosity may play a more crucial role in the hardness .

Table 3 Mechanical properties of pure and doped CS after sintering at 1200°C for 2h.

| Composite Name | Hardness (GPa) | Fracture Toughness (MPa $m^{1/2}$) | Young's Modulus (GPa) |
|---|---|---|---|
| **CS** | 2.57±0.13 | 0.67±0.06 | 105.3±6.1 |
| **TCS5** | 7.01±0.14 | 1.51±0.05 | 133.5±5.1 |
| **TCS10** | 5.10±0.0.38 | 1.17±0.09 | 121.2±7.1 |
| **TCS15** | 3.28±0.27 | 1.14±0.01 | 118.4±5.4 |
| **ACS5** | 4.30±0.47 | 0.99±0.09 | 111.6±3.2 |
| **ACS10** | 4.52±0.31 | 1.07±0.01 | 110.3±4.6 |
| **ACS15** | 4.91±0.17 | 1.05±0.02 | 107.2±4.9 |

In the ACS samples it appeared that a higher amount of dopant and combined with the standard temperature profile of the sintering process increased the flow of ions, which resulted in the closure of surface porosity, which is called the "filling in" effect[49]. The effect entails that exposed surfaces are the hottest part of a sample. The comparatively small differences (within the margin of error) in the hardness values between the different ACS specimens could be due to only insignificant variations in the open porosity of ACS samples.

TCS specimens show a different behavior from ACS. TCS5 shows the highest value of hardness among the TCS specimens. With incorporation of 5 wt% Ta, the hardness increased to 7.01±0.1 which is 2.7 times more than pure CS. With increasing amounts of Ta, the hardness values decreased again dramatically due to the reduction in density of the samples. Although it was expected that the "filling in" effect would be observed for all TCS specimens, this was not the case. Apparently the difference in temperature between surface and interior did not lead to significant lower surface porosity for TCS10 and TCS15.

The doped bioceramics certainly had higher values of fracture toughness and hardness (Table 3), than pure CS (fracture toughness of pure CS was 0.67±0.06 MPa $m^{1/2}$). In spite of the similar microstructures

and grain sizes of Ag and Ta doped CS sintered at 1200°C, the Ta doped bioceramics had higher fracture toughness, as a consequence of the more extensive phase transformation of α to β-CS in the case of the Ag doped CS. In the case of TCS specimens, with Ta content of 5 wt% showed a 105% increase in fracture toughness, which could be interpreted as a lowering of the amounts of α phase, which is the phase with the lower fracture toughness.

Improving the fracture toughness of the doped samples was not limited to the phase transition and grain size but extended to the relative density. Consequently, although undoped CS samples had a biphasic structure they had the lowest fracture toughness. In addition to the biphasic structure, TCS5 specimens had the highest value of relative density, which in turn was a strong reason for a higher fracture toughness. With the decrease in density for the other TCS samples, the fracture toughness value was decreased by about 50%.

However TCS10 and TCS15 had nearly the same fracture toughness even though they had different phase structures. This could be due to the similar relative densities of TCS10 and TCS15.

Contrary to Ta doping, the level of Ag doping did not have a significant effect on the fracture toughness of ACS specimens. With addition of Ag the fracture toughness increased around 30% compared to undoped CS. ACS5 and ACS10 have a monophasic structure of α-CS even though in ACS15 some β-CS was observed. Based on the crystallinity study it was expected that ACS15 samples showed higher fracture toughness values. However, considering the relative densities of ACS specimens it could be claimed that the higher density of ACS15 could moderate the rate of changes in regards to the fracture toughness.

The elastic modulus of pure CS in the biphasic structure of α- and β-CS was 105±6 GPa, which increased to 134±5 GPa for TCS5. The increase of the elastic modulus of TCS5 could be due to the higher relative density, and smaller grain size in comparison with other specimens [50]. This explains the reduction of the elastic modules of TCS10 and TCS15 specimens. With increasing amounts of Ta in the CS structure, the Young's modulus decreased to values of 121±7 GPa and 118±5 GPa for TCS10 and TCS15 respectively.

In ACS samples, lower elastic modulus values were observed than in TCS. In ACS5 the elastic modulus decreased to 112±3 GPa due to lower relative density compared to TCS5. This value did not change significantly for ACS10 (110±5 GPa) and ACS15 (107±5 GPa) samples.

### 3.3 Apatite forming on the surface of the samples

Selected samples were immersed in SBF in order to analyze their ability to form the apatite layers on their surface. The XRD patterns of doped and undoped CS samples after soaking in SBF for 14 d are presented in Figure 3. Only the characteristic reflections of apatite (According to JCPDS 24-0033) existed in the XRD pattern and there was no difference in the intensity of reflections with different Ag and Ta contents in the CS lattice.

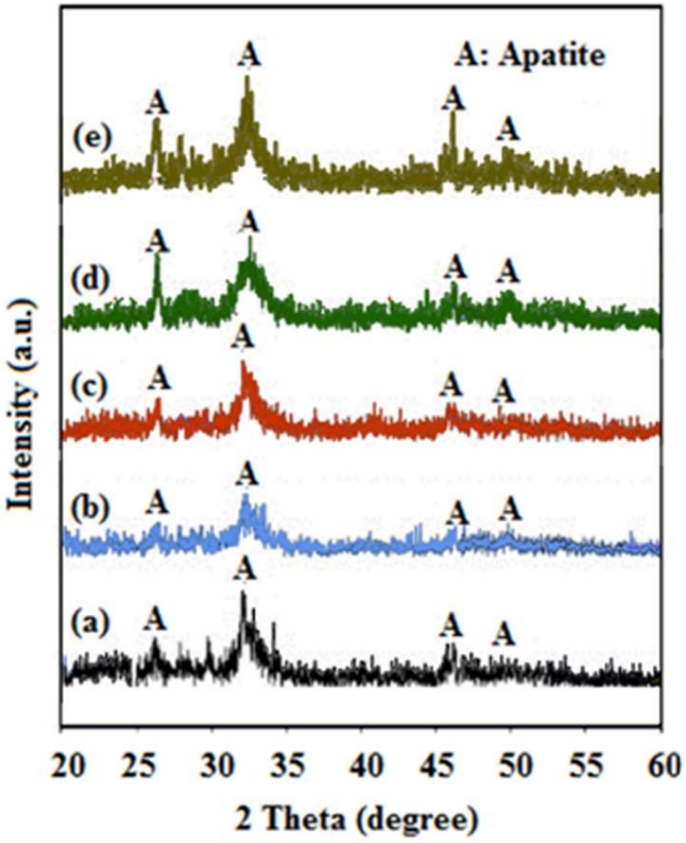


Figure 3 XRD patterns of apatite formation on the surface of the (a) pure CS, (b) ACS5, (c) ACS10, (d) TCS5, (e) TCS10 after soaking in SBF for 14 days.

Another result which can be obtained from the XRD patterns was that all specimens were fully covered by HA layers after incubation in SBF for 14 days, which demonstrated the ability of all doped and undoped CS samples to form apatite on their surfaces. Furthermore, no calcite peaks were observed in the XRD patterns; calcite could have side effects in biomedical engineering applications when performing *in vivo* tests.

There was no significant difference between the morphology of pure and doped CS specimens. For all FESEM micrographs show the apatite layer that was formed on the pure and doped CS ceramics (Figure 4). For all specimens it could be observed that the apatite layers had a flake-like structure, where the crystal boundaries were evident. EDX spectrum analyses (Figure 4) confirmed the formation of apatite layers on the surface of the pure and doped samples.

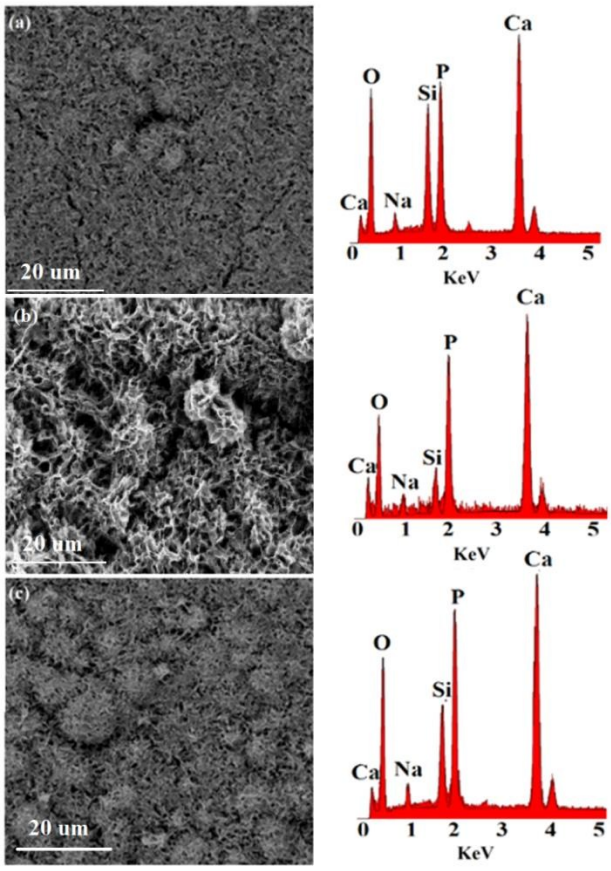


Figure 4 Apatite formation (left) and EDX spectrum (right) of the (a) Pure CS (b) ACS10 and (c) TCS10 after incubation in SBF for 14 days.

In the present study, the incorporation of Ag and Ta in the CS structure decreased the release of Si ions into SBF resulting in an overall reduction in the dissolution of the CS bioceramic. Incorporation of $Ag^{+}$ and $Ta^{5+}$ enhances the density of CS ceramics, as it was previously discussed, and the higher density lower degradation [51]. Further, $Ag^{+}$ has a larger radius than $Ca^{2+}$, which occupies more space in the crystal lattice and inhibits the movement and release of silicate anions and thereby decreases the dissolution rate of CS.

$Ta^{5+}$ has a smaller ion radius than $Ca^{2+}$, which provides more vacancies in the structure of CS leading to more ions being released and consequently a higher degradation rate of CS. This explains why the Si peak was more intensive in the EDX spectrum of ACS10 than TCS10. The ratio of Ca/P for Ag and Ta doped CS was 1.54, which was less than stoichiometric of HA (1.67). This was likely due to release of metallic cations into the SBF, which decreased the pH of the solution and finally lead to formation of another kind of calcium phosphate crystal; tricalcium phosphate (TCP), which was formed at a lower pH than hydroxyapatite [52].

### 3.4 Ion release into the SBF solution

The Ca and Si ions concentrations in SBF solution after incubating the selected doped and undoped samples were determined to assess the effect of doping on the ion release of the sintered specimens. As presented in Figure 5, higher amounts of calcium ions were released from undoped CS than from ACS10 and TCS10. This is due to the higher amount of Ca ions in the lattice of CS, i.e. a smaller amount of Ca in the material leads to smaller amount of Ca ions release into the SBF solution.

In case of silicon ions, the higher density of ACS and TCS samples resulted in a stronger bonding in the structure of CS leading to reduction of ion release in the SBF solution. Since the ion radius of Ag ion is larger than Ca ion it can occupy more vacancies in the lattice of CS bringing about reduction of ion movement and consequently reduced the release of Si ions into the SBF solution. On the other hand, the presence of Ta ion in the CS lattice created more spaces, which could boost ion release from the structure in comparison to the Ag doped specimens. However, the amount of Ta could weaken the crystal structure

compared to pure CS. This was counteracted by the higher degree of densification effected by the Ta onto the doped CS structure, which prevented the release of ions in large quantities.

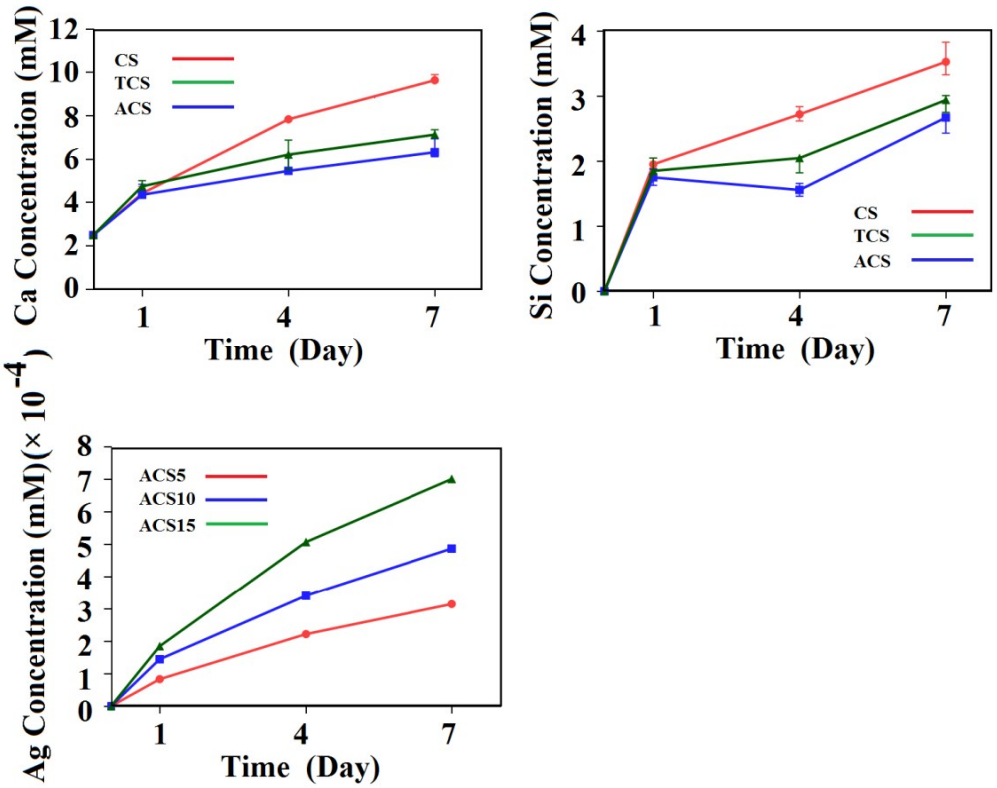


Figure 5 Ion release from pure CS, ACS10 and TCS10.

Figure 5 also demonstrated that release of Ag ions into SBF solution increased from day one to day 7 as well as higher concentration of Ag into the CS lattice. The amount release of Ag ions from all ACS samples is less than $8\times10^{-4}$ mM. Silver has a bactericidal activity at concentrations as low as $3.5\times10^{-4}$ mM without toxic effects to mammalian cells. In vivo, silver levels below $2\times10^{-3}$ mM in the blood were considered normal because every day humans ingest small amounts of silver, small amounts of which are resorbed by the intestine, the rest (majority) being excreted by the liver[53].

The pH value of Ta and Ag containing CS ceramics-soaked solution was lower compared to pure CS ceramics (Figure 6). Release of Ca and Si ions from CS into the solution can increase the pH value. The most important and interesting is that when bone forms, the crosslinking of the collagen chains and

the subsequent precipitation of hydroxyapatite are pH dependent and require an optimally pH at the bone formation site [41]. Our results showed that the ACS and TCS samples decreased the pH value in SBF, suggesting a potential preferable material for *in vitro* bone cell culture. On the other hand, even in higher concentrations of Ta and Ag, the pH value was not decreased to lower than 7.3 indicating there was no concern about acidification of SBF solution.

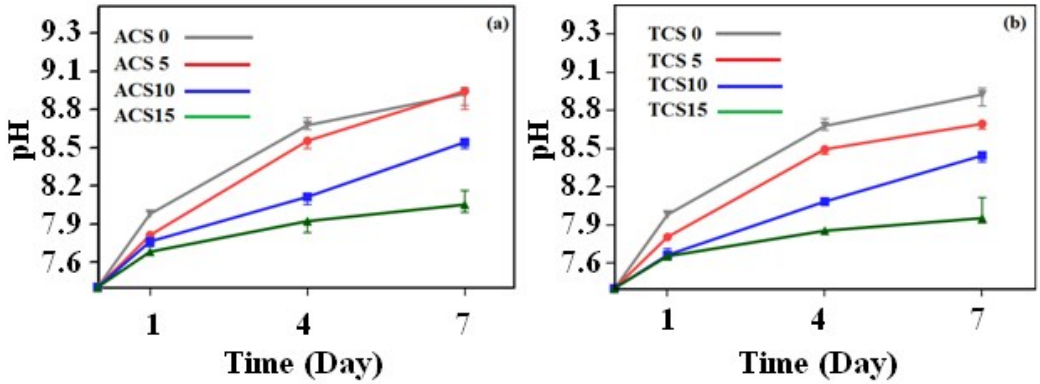


Figure 6 pH changes of (a) ACS and (b) TCS samples in SBF solution for different soak-time.

### 3.5 Cell proliferation and MTT assay of pure and doped CS

hFOB cell proliferations on undoped and Ag-/Ta- doped CS specimens were determined by MTT assay. Figure 7 shows that the cells proliferated on all of the ACS, TCS and pure CS samples significantly from day 3 to day 7. In comparison, cell density did not increase from day 1 to 3. On day 3, there was no statistically significant difference in all densities between CS, ACS and TCS. Even on day 7, when hFOB cells significantly proliferated on all samples the difference between the samples was small.

Cellular attachment and growth of the hFOB cells on the pure CS, ACS and TCS specimens were analyzed by FESEM. Figure 8 shows the cellular morphology and attachment behavior on the surfaces of pure and doped CS after 1 day of culturing. As can be seen in the Figures 8a-c, hFOB cells spontaneously attached to the surfaces with osteoblast phenotype extensions.

As Ag is extensively used as antimicrobial agent, concerns regarding its cytocompatibility have been raised[53-54] . MTT results (Figure 7a) showed no significant negative effect on cellular proliferation on

samples incorporating Ag due to lack of solubility. It must be noted that most of the reports regarding the cytotoxicity of silver have been related to the incorporation of silver oxide ($Ag_2O$) in the structure of bioactive ceramics such as HA.

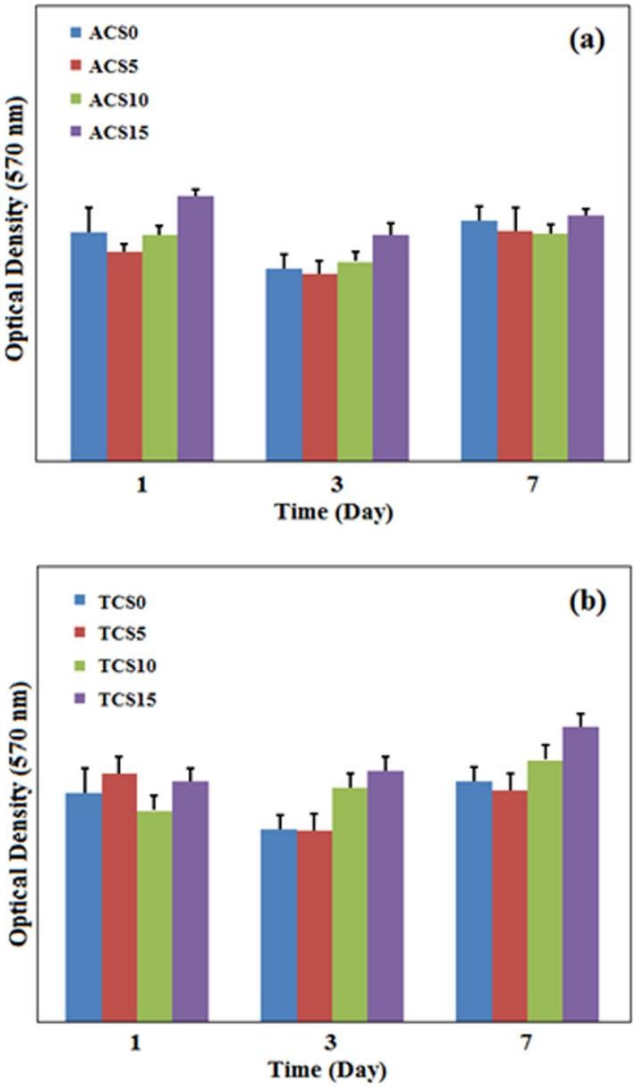


Figure 7 MTT assay of hFOB cells cultured on the pure and doped CS samples.

Ag can create hydroxyl radicals (·OH) and superoxide anions ($O_2^-$) by photocatalytic reactions, which can lead to protein inactivation and eventual cell apoptosis [55-56] which by proper doping of Ag cation in the lattice of CS, this problem can be greatly remedied. A small decrease in cell proliferation of ACS15

compared from day 1 to day 7 may indicate that an amount of Ag higher than 15% might increase the cytotoxicity.

With incorporation of tantalum in the structure of CS, the cell proliferation was increased at each time point (Figure 7b). With increasing the amount of Ta in the lattice of CS, the MTT assay showed a slight increase in cell proliferation, which confirmed that Ta has a higher bioactivity than Ag. Cell attachment and growth were primarily associated with material surface characteristics such as wettability and surface energy.

A higher release of silicate and Ca ions into the cell culture medium could promote cell proliferation in the presence of TCS. On TCS extra cellular matrix (ECM) was secreted by the seeded hFOB cells and the cells merged on the surface of the samples to form cell layers. Merging induced the formation of a rich ECM indicative of high cell activity on TCS compared to ACS samples. Since bone is produced by the mineralization of an organic matrix (largely collagen) through the nucleation and growth of a mineral similar to HA, the presence of calcium phosphate in the ECM acts as a key factor in the regulation of bone remodeling and cartilage [57].

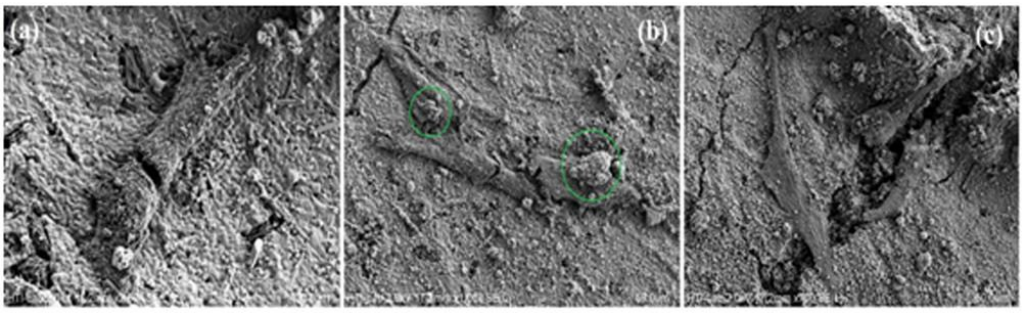


Figure 8 FESEM images of hFOB Cells attachment to the surface of the (a) pure CS, (b) TCS10 and (c) ACS10 samples after 1 day cell seeding.

## 4. Conclusion

5. The presented results indicate that CS doped with Ta and Ag shows improved mechanical and altered biological properties. 5 wt% Ta incorporation into CS lattice resulted in enhanced hardness and fracture

toughness values, significantly more so than 5% Ag. Higher Ta contents led to a decrease in the hardness and fracture toughness, while a higher amount of Ag had no obvious further effect on the mechanical properties. Both Ta and Ag doped CS could form surface apatite on immersion in simulated body fluid. Incorporation of Ta into the CS stimulated hFOB cell proliferation, i.e. for higher amounts of Ta, the proliferation was increased. However, increasing the concentration of Ag to 15% decreased cell proliferation in comparison to lower amounts of Ag and compared to doping silicates with Ta.

**Acknowledgement**

This work was supported by Ministry of Higher Education of Malaysia (MOHE), Project number "D000014-16001" (Synthetic Prosthetic socket through stump-liner interfacial stresses measurement), as well as grant numbers "UMRG RP021-2012A" and "FRGS FP007-2013A".

**Notes**

The authors declare no competing financial interest. First and second authors have equally contributed to this work.

## References


1. Hench, L. L.; Wilson, J.; McLaren, M.; Niesz, D., *An introduction to bioceramics*. World Scientific Singapore: **1993**; Vol. 1.
2. Liu, X.; Morra, M.; Carpi, A.; Li, B., Bioactive calcium silicate ceramics and coatings. *Biomedicine & Pharmacotherapy* **2008,** *62* (8), 526-529.
3. Shirazi, S. F. S.; Gharehkhani, S.; Mehrali, M.; Yarmand, H.; Metselaar, H. S. C.; Kadri, N. A.; Osman, N. A. A., A review on powder-based additive manufacturing for tissue engineering: selective laser sintering and inkjet 3D printing. *Science and Technology of Advanced Materials* **2015,** *16* (3), 033502.
4. De Aza, P.; Guitian, F.; De Aza, S., Bioactivity of wollastonite ceramics: in vitro evaluation. *Scripta metallurgica et materialia* **1994,** *31* (8), 1001-1005.
5. De Aza, P.; Guitian, F.; De Aza, S., Bioeutectic: a new ceramic material for human bone replacement. *Biomaterials* **1997,** *18* (19), 1285-1291.
6. Hench, L.; Paschall, H., Histochemical responses at a biomaterial's interface. *Journal of biomedical materials research* **1974,** *8* (3), 49-64.
7. Xue, W.; Liu, X.; Zheng, X.; Ding, C., In vivo evaluation of plasma-sprayed wollastonite coating. *Biomaterials* **2005,** *26* (17), 3455-3460.
8. Shirazi, F. S.; Mehrali, M.; Oshkour, A. A.; Metselaar, H. S. C.; Kadri, N. A.; Abu Osman, N. A., Characterization and Mechanical Properties of Calcium Silicate/Citric Acid–Based Polymer Composite Materials. *International Journal of Applied Ceramic Technology* **2015,** *12* (2), 371-376.
9. Shirazi, F. S.; Moghaddam, E.; Mehrali, M.; Oshkour, A. A.; Metselaar, H. S. C.; Kadri, N. A.; Zandi, K.; Abu, N. A., In vitro characterization and mechanical properties of β-calcium silicate/POC composite as a bone fixation device. *Journal of Biomedical Materials Research Part A* **2014,** *102* (11), 3973-3985.
10. Shirazi, F.; Mehrali, M.; Oshkour, A.; Metselaar, H.; Kadri, N.; Abu Osman, N., Mechanical and physical properties of calcium silicate/alumina composite for biomedical engineering applications. *Journal of the Mechanical Behavior of Biomedical Materials* **2014,** *30*, 168-175.
11. Gharehkhani, S.; Shirazi, S. F. S.; Jahromi, S. P.; Sookhakian, M.; Baradaran, S.; Yarmand, H.; Oshkour, A. A.; Kazi, S. N.; Basirun, W. J., Spongy nitrogen-doped activated carbonaceous hybrid derived from biomass material/graphene oxide for supercapacitor electrodes. *RSC Advances* **2015,** *5* (51), 40505-40513.
12. Shirazi, S. F. S.; Gharehkhani, S.; Yarmand, H.; Badarudin, A.; Metselaar, H. S. C.; Kazi, S. N., Nitrogen doped activated carbon/graphene with high nitrogen level: Green synthesis and thermo-electrical properties of its nanofluid. *Materials Letters* **2015,** *152*, 192-195.
13. Nasiri-Tabrizi, B.; Pingguan-Murphy, B.; Basirun, W. J.; Baradaran, S., Crystallization behavior of tantalum and chlorine co-substituted hydroxyapatite nanopowders. *Journal of Industrial and Engineering Chemistry* **2015**.
14. Webster, T. J.; Ergun, C.; Doremus, R. H.; Bizios, R., Hydroxylapatite with substituted magnesium, zinc, cadmium, and yttrium. II. Mechanisms of osteoblast adhesion. *Journal of biomedical materials research* **2002,** *59* (2), 312-317.
15. Webster, T. J.; Massa-Schlueter, E. A.; Smith, J. L.; Slamovich, E. B., Osteoblast response to hydroxyapatite doped with divalent and trivalent cations. *Biomaterials* **2004,** *25* (11), 2111-2121.
16. Kalaivani, S.; Singh, R. K.; Ganesan, V.; Kannan, S., Effect of copper (Cu 2+) inclusion on the bioactivity and antibacterial behavior of calcium silicate coatings on titanium metal. *Journal of Materials Chemistry B* **2014,** *2* (7), 846-858.
17. Stanić, V.; Janaćković, D.; Dimitrijević, S.; Tanasković, S. B.; Mitrić, M.; Pavlović, M. S.; Krstić, A.; Jovanović, D.; Raičević, S., Synthesis of antimicrobial monophase silver-doped hydroxyapatite nanopowders for bone tissue engineering. *Applied Surface Science* **2011,** *257* (9), 4510-4518.

18. Hidalgo, E.; Domınguez, C., Study of cytotoxicity mechanisms of silver nitrate in human dermal fibroblasts. *Toxicology letters* **1998,** *98* (3), 169-179.
19. Brandt, D.; Park, B.; Hoang, M.; Jacobe, H. T., Argyria secondary to ingestion of homemade silver solution. *Journal of the American Academy of Dermatology* **2005,** *53* (2), S105-S107.
20. Hu, C.; Guo, J.; Qu, J.; Hu, X., Efficient destruction of bacteria with Ti (IV) and antibacterial ions in co-substituted hydroxyapatite films. *Applied Catalysis B: Environmental* **2007,** *73* (3), 345-353.
21. Balla, V. K.; Bodhak, S.; Bose, S.; Bandyopadhyay, A., Porous tantalum structures for bone implants: Fabrication, mechanical and in vitro biological properties. *Acta Biomaterialia* **2010,** *6* (8), 3349-3359.
22. Ligot, S.; Godfroid, T.; Music, D.; Bousser, E.; Schneider, J. M.; Snyders, R., Tantalum-doped hydroxyapatite thin films: Synthesis and characterization. *Acta Materialia* **2012,** *60* (8), 3435-3443.
23. Shuai, C.; Gao, C.; Feng, P.; Peng, S., Graphene-reinforced mechanical properties of calcium silicate scaffolds by laser sintering. *RSC Advances* **2014,** *4* (25), 12782-12788.
24. Baradaran, S.; Moghaddam, E.; Basirun, W. J.; Mehrali, M.; Sookhakian, M.; Hamdi, M.; Moghaddam, M. R. N.; Alias, Y., Mechanical properties and biomedical applications of a nanotube hydroxyapatite-reduced graphene oxide composite. *Carbon* **2014,** *69* (0), 32-45.
25. Zhang, X.; Gubbels, G. M.; Terpstra, R.; Metselaar, R., Toughening of calcium hydroxyapatite with silver particles. *Journal of materials science* **1997,** *32* (1), 235-243.
26. Rameshbabu, N.; Sampath Kumar, T.; Prabhakar, T.; Sastry, V.; Murty, K.; Prasad Rao, K., Antibacterial nanosized silver substituted hydroxyapatite: synthesis and characterization. *Journal of Biomedical Materials Research Part A* **2007,** *80* (3), 581-591.
27. Meyssamy, H.; Riwotzki, K.; Kornowski, A.; Naused, S.; Haase, M., Wet-Chemical Synthesis of Doped Colloidal Nanomaterials: Particles and Fibers of LaPO4: Eu, LaPO4: Ce, and LaPO4: Ce, Tb. *Advanced Materials* **1999,** *11* (10), 840-844.
28. Huang, K.; Goodenough, J. B., Wet Chemical Synthesis of Sr-and Mg-Doped LaGaO< sub> 3</sub>, a Perovskite-Type Oxide-Ion Conductor. *Journal of Solid State Chemistry* **1998,** *136* (2), 274-283.
29. Zamiri, R.; Singh, B.; Dutta, D.; Reblo, A.; Ferreira, J., Electrical properties of Ag-doped ZnO nano-plates synthesized via wet chemical precipitation method. *Ceramics International* **2014,** *40* (3), 4471-4477.
30. Ma, Z.; Shao, G.; Wang, G.; Du, J.; Zhang, Y., Electrochemical performance of Mo-doped LiFePO4/C composites prepared by two-step solid-state reaction. *Ionics* **2013,** *19* (3), 437-443.
31. Han, S.; Jang, T.-H.; Kim, Y.; Park, B.-G.; Park, J.-H.; Jeong, Y., Magnetism in Mn-doped ZnO bulk samples prepared by solid state reaction. *Applied Physics Letters* **2003,** *83* (5), 920-922.
32. Suryanarayana, C., Mechanical alloying and milling. *Progress in materials science* **2001,** *46* (1), 1-184.
33. Baláž, P.; Achimovičová, M.; Baláž, M.; Billik, P.; Cherkezova-Zheleva, Z.; Criado, J. M.; Delogu, F.; Dutková, E.; Gaffet, E.; Gotor, F. J., Hallmarks of mechanochemistry: from nanoparticles to technology. *Chemical Society Reviews* **2013,** *42* (18), 7571-7637.
34. Shirazi, F. S.; Mehrali, M.; Nasiri-Tabrizi, B.; Baradaran, S.; Gharehkhani, S.; Metselaar, H.; Kadri, N.; Osman, N. A., Mechanochemical Synthesis and Characterization of Silver (Ag) and Tantalum (Ta5+) Doped Calcium Silicate Nanopowders. *Science of Advanced Materials* **2015,** *7* (12).
35. Nasiri-Tabrizi, B.; Adhami, T.; Ebrahimi-Kahrizsangi, R., Effect of processing parameters on the formation of TiB2 nanopowder by mechanically induced self-sustaining reaction. *Ceramics International* **2014,** *40* (5), 7345-7354.
36. Anstis, G. R.; Chantikul, P.; Lawn, B. R.; Marshall, D. B., A Critical Evaluation of Indentation Techniques for Measuring Fracture Toughness: I, Direct Crack Measurements. *Journal of the American Ceramic Society* **1981,** *64* (9), 533-538.

37. Lawn, B. R.; Evans, A. G.; Marshall, D. B., Elastic/Plastic Indentation Damage in Ceramics: The Median/Radial Crack System. *Journal of the American Ceramic Society* **1980,** *63* (9-10), 574-581.
38. Shetty, D. K.; Wright, I. G.; Mincer, P. N.; Clauer, A. H., Indentation fracture of WC-Co cermets. *Journal of Materials Science* **1985,** *20* (5), 1873-1882.
39. Kokubo, T., Surface chemistry of bioactive glass-ceramics. *Journal of Non-Crystalline Solids* **1990,** *120* (1–3), 138-151.
40. Wu, C. T.; Ramaswamy, Y.; Kwik, D.; Zreiqat, H., The effect of strontium incorporation into CaSiO3 ceramics on their physical and biological properties. *Biomaterials* **2007,** *28* (21), 3171-3181.
41. Wu, C. T.; Zreiqat, H., Preparation and characteristics of strontium containing bioactive CaSiO3 ceramics. *Key Engineering Materials* **2007,** *330*, 499-502.
42. Okada, K.; Yamamoto, N.; Kameshima, Y.; Yasumori, A.; MacKenzie, K. J. D., Effect of Silica Additive on the Anatase-to-Rutile Phase Transition. *Journal of the American Ceramic Society* **2001,** *84* (7), 1591-1596.
43. Cho, J.-H.; Park, I.-K.; Kim, H.-G.; Chung, H.-T., Sintering Behavior of Cadmium-Doped Pb(Ni1/3Nb2/3)O3–PbZrO3–PbTiO3 Ceramics. *Journal of the American Ceramic Society* **1997,** *80* (6), 1523-1534.
44. Naga, S. M.; Hassan, A. M.; Awaad, M.; Bondioli, F., Influence of Ta 2 O 5 Doping on the Microstructure, Physical and Mechanical Properties of a-Alumina Ceramics. *journal of ceramic science and technology* **2013,** *4* (4), 187-192.
45. Rani, D. A.; Yoshizawa, Y.; Hirao, K.; Yamauchi, Y., Effect of Rare-Earth Dopants on Mechanical Properties of Alumina. *Journal of the American Ceramic Society* **2004,** *87* (2), 289-292.
46. Chen, P.-L.; Chen, I. W., Role of Defect Interaction in Boundary Mobility and Cation Diffusivity of CeO2. *Journal of the American Ceramic Society* **1994,** *77* (9), 2289-2297.
47. Luo, J., and R. Stevens., Porosity-dependence of elastic moduli and hardness of 3Y-TZP ceramics. Ceramics International 1999, 25(3), 281-286.
48. Curran, D. J.; Fleming, T. J.; Towler, M. R.; Hampshire, S., Mechanical parameters of strontium doped hydroxyapatite sintered using microwave and conventional methods. *Journal of the Mechanical Behavior of Biomedical Materials* **2011,** *4* (8), 2063-2073.
49. Melnick, C.; Chen, Z.; Mecholsky, J., Hardness and toughness of exoskeleton material in the stone crab, Menippe mercenaria. *Journal of materials research* **1996,** *11* (11), 2903-2907.
50. Zhao, X. J.; Chen, D. L.; Ru, H. Q.; Zhang, N., Zirconium nitride nano-particulate reinforced Alon composites: Fabrication, mechanical properties and toughening mechanisms. *J. Eur. Ceram. Soc.* **2011,** *31* (5), 883-892.
51. Li, J.; Liao, H.; Hermansson, L., Sintering of partially-stabilized zirconia and partially-stabilized zirconia—hydroxyapatite composites by hot isostatic pressing and pressureless sintering. *Biomaterials* **1996,** *17* (18), 1787-1790.
52. Chen, Y. P.; Rekha, P. D.; Arun, A. B.; Shen, F. T.; Lai, W. A.; Young, C. C., Phosphate solubilizing bacteria from subtropical soil and their tricalcium phosphate solubilizing abilities. *Applied Soil Ecology* **2006,** *34* (1), 33-41.
53. Ewald, A.; Hösel, D.; Patel, S.; Grover, L. M.; Barralet, J. E.; Gbureck, U., Silver-doped calcium phosphate cements with antimicrobial activity. *Acta Biomaterialia* **2011,** *7* (11), 4064-4070.
54. Zare-Zardini, H.; Amiri, A.; Shanbedi, M.; Taheri-Kafrani, A.; Kazi, S. N.; Chew, B. T.; Razmjou, A., In vitro and in vivo study of hazardous effects of Ag nanoparticles and Arginine-treated multi walled carbon nanotubes on blood cells: Application in hemodialysis membranes. *Journal of Biomedical Materials Research Part A* **2015,** *103* (9), 2959-2965.
55. Song, W.-H.; Ryu, H. S.; Hong, S.-H., Antibacterial properties of Ag (or Pt)-containing calcium phosphate coatings formed by micro-arc oxidation. *J. Biomed. Mater. Res. Part A* **2009,** *88A* (1), 246-254.

56. Sunada, K.; Watanabe, T.; Hashimoto, K., Studies on photokilling of bacteria on TiO2 thin film. *Journal of Photochemistry and Photobiology A: Chemistry* **2003,** *156* (1–3), 227-233.
57. Kumar, A.; Biswas, K.; Basu, B., Hydroxyapatite-titanium bulk composites for bone tissue engineering applications. *J. Biomed. Mater. Res. Part A* **2015,** *103* (2), 791-806.